Available online at www.sciencedirect.com
SCIENCE DIRECT®
European Journal of Medicinal Chemistry 39 (2004) 835–847
EUROPEAN JOURNAL OF MEDICINAL CHEMISTRY
www.elsevier.com/locate/ejmech

Original article

Investigation of structure–activity relationships in a series of glibenclamide analogues

Elizabeth Yuriev [a], David C.M. Kong [b], Magdy N. Iskander [a,*]

[a] Department of Medicinal Chemistry, Victorian College of Pharmacy, Monash University, 381 Royal Parade, Parkville 3052, Victoria, Australia
[b] Department of Pharmacy Practice, Victorian College of Pharmacy, Monash University, 381 Royal Parade, Parkville 3052, Victoria, Australia

Received 24 July 2003; received in revised form 11 June 2004; accepted 14 June 2004

Available online 23 July 2004

Abstract

In this study, the synthesis of 15 new glibenclamide analogues is described. The conformational trends of these analogues were investigated using Monte Carlo conformational analysis. The conformational analysis results resolved the discrepancy between previous molecular modelling simulations of glibenclamide and allowed rationalizing the effect of aqueous environment on the overall conformation. The 3D-QSAR study was carried out with respect to the compounds' ability to antagonize the [^{3}H]-glibenclamide binging in rat cerebral cortex. Superimposition of the antagonists was performed using the conformations derived from atom-by-atom fit to the glibenclamide crystal structure and this alignment was used to develop CoMFA models. CoMFA provided a good predictability: number of PLS components = 2, $q^2 = 0.876$, $R^2 = 0.921$, SEE = 0.455 and $F = 70$. Best CoMFA models showed the steric and lipophilic properties as the major interacting forces whilst the electrostatic property contribution was a minor factor.

Keywords: CoMFA; Conformational analysis; Glibenclamide; K_{ATP} channel

1. Introduction

Developing new K^+ antagonists for K_{ATP}-channels [1] is a challenging area of drug design with research in this field growing exponentially. It is anticipated that these molecules will have considerable therapeutic value in diabetes and cardiac dysfunction [2].

Glibenclamide (Fig. 1) is a potent and selective K_{ATP} channel blocker and a potent oral hypoglycaemic agent [2–4]. It is a member of the sulfonylurea family and has a high affinity inhibition of the K_{ATP}-Kir 6.2 (subfamily) sulfonylurea binding site, which appears to be important for K_{ATP} channel regulation [5]. The mechanism of action of the drug consists of the interaction with a sulfonylurea receptor (SUR) and the inhibition of the ATP-sensitive K^+ channel, which depolarizes the cells and leads to insulin secretion [1,6,7]. The same mechanism of drug action is at play at the extrapancreatic sites in the liver, kidney, brain, skeletal, heart, and smooth muscle [3,6,8–11]. Despite the wide acceptance of glibenclamide and several other sulfonylurea drugs, several risks limit their applications [3,12]. Specifically, sulfonylureas are associated with: hypoglycemia and weight gain; hyperinsulinemia and thus a deterioration in diabetes; the increasing the risk of cardiovascular mortality (in long-term treatment) [13–15].

Previously, we had tested glibenclamide and analogues for their ability to antagonize the vasorelaxant actions of the K^+ channel opener levcromakalim in rat thoracic aorta and to displace [^{3}H]-glibenclamide from rat cerebral cortex membranes [16]. That study demonstrated that glibenclamide and analogues were active as antagonists of levcromakalim-mediated responses. Our glibenclamide analogues were also 1000 to 10,000 times more potent at displacing [^{3}H]-glibenclamide from rat cerebral cortex membranes. The results also revealed the quantitative differences in the activities of the sulfonamide/sulfonylurea-based compounds studied. Specifically, the sulfonamide analogues had a more dramatic effect as levcromakalim antagonists than as agents that displace [^{3}H]-glibenclamide. Therefore, the main finding from that study was that the above two propensities of glibenclamide analogues are based on different structure–

* Corresponding author. Tel.: +61-3-99039545; fax: +61-3-99039582.
E-mail address: magdy.iskander@vcp.monash.edu.au (M.N. Iskander).

doi:10.1016/j.ejmech.2004.06.004

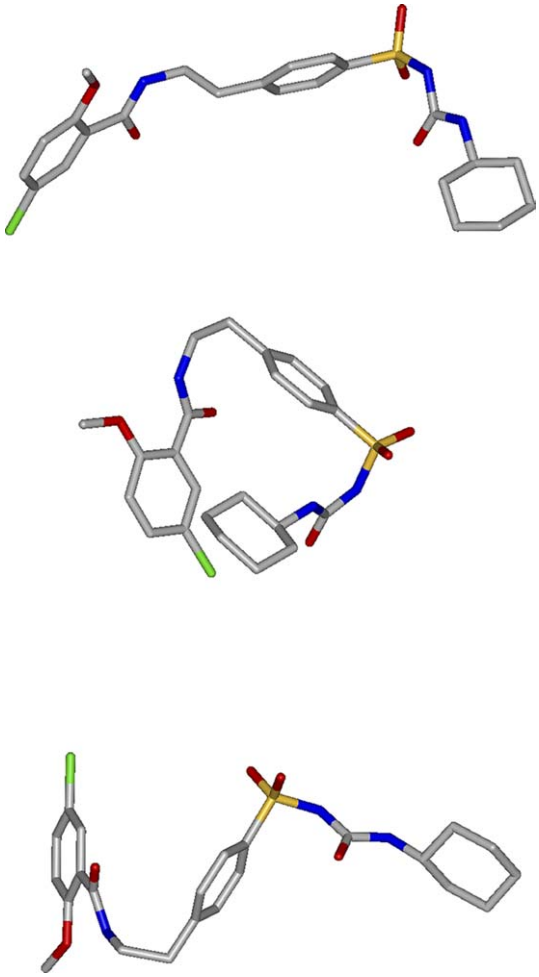

Fig. 1. 3D structure of glibenclamide. Hydrogens are omitted for clarity. Colour coding: C, grey; O, red; N, blue; S, yellow; Cl, green. (Top) Crystal structure [17]. Coordinates are taken from CSD (refcode DUNXAL). (Middle) Lowest energy conformation resulting from the systematic conformational search in vacuo. (Bottom) Lowest energy conformation resulting from the systematic conformational search in explicit aqueous solution.

activity relationships (SARs). It has been also shown that different structure–activity relationships exist for different structural groups of analogues (i.e., amidoethylbenzenesulphonylureas, sulphonamides, benzenesulphonylureas, benzamide, benzoylcyclohexylureas, and benzoylphenylthioureas).

Such differentiation may be important for developing better compounds with greater specificity in antagonistic activity. The aim of the current study was therefore to analyse the three-dimensional (3D) structural properties of a number of closely related glibenclamide analogues in order to clarify the structure–activity relationships in quantitative terms and to assess the relative contributions of different structural elements to the antagonistic activity. In particular, conformational analysis and Comparative Molecular Field Analysis (CoMFA) study of these compounds have been carried out. Detailed conformational analysis, now carried out both in vacuo and in explicit aqueous solution, provides data complementary to previously published NMR and X-ray investigations of glibenclamide [17]. It also allows us to critically revisit the conclusions of earlier reported conformational studies of glibenclamide [18–20]. CoMFA models as well as CoMFA predictions for modified analogues confirmed the importance of several structural elements for the K_{ATP} channel blocking activity and allowed arriving at a set of rules for the design of new compounds with improved activity.

2. Chemistry and pharmacology

Amidoethylbenzenesulphonamides **1a–h** and amidoethylbenzenesulphonylureas **2b–h** were synthesized as outlined in Scheme 1. Benzenesulphonylureas **4a–d** were synthesized as outlined in Scheme 2. Drugs that were generously donated (Scheme 3) were: glibenclamide **2a** (Hoechst Pharmaceutical Co., Melbourne, Australia), glipizide **2i** (Farmitalia Carlo Erba, Milan, Italy), iodoglibenclamide **2j** (from Dr. Donald Gehlert, Lilly Research Laboratories, Indianapolis, IN). Benzamide 5 (Scheme 3) was prepared by a procedure similar to that outlined for amidoethylbenzenesulphonamides **1a–h** in Scheme 1. The measurement of the pK_i values of the inhibition of [^{3}H]-glibenclamide binding in rat cerebral cortex by these compounds (Table 1) was described elsewhere [16].

3. Results and discussion

3.1. Conformational analysis

In order to further elucidate glibenclamide mechanism of action and to develop more potent agents free of the limitations mentioned in the introduction, the structural information relating to the SUR–glibenclamide interaction is necessary. Unfortunately, no 3D structural data is available with respect to this interaction. The lack of such information leaves structural investigation of isolated glibenclamide as the main line of attack aimed at determination of biologically relevant conformation(s).

Previously, conformational preferences of glibenclamide have been studied experimentally by NMR and X-ray crystallography [17]. It has been shown that, in the solid state, glibenclamide exhibits an extended conformation (Fig. 1, top). In the same investigation, the conformational behaviour of glibenclamide was studied in solution and the free rotation around bonds t2 and t3 (as designated in Fig. 2) was demonstrated.

Conformational trends of glibenclamide analogues have also been a subject of molecular mechanics studies [18–20], which resulted in contradictory conclusions. While Grell et al. [20] generated the lowest energy structure with the conformation identical to that in the solid state, Lins et al. [18,19] produced lowest energy structures displaying a U-shaped conformation with hydrophobic cycles at the extremity of each branch and a peptidic bond at the bottom of the U.

Thus, we undertook to carry out a detailed conformational analysis of the glibenclamide system in order to achieve a

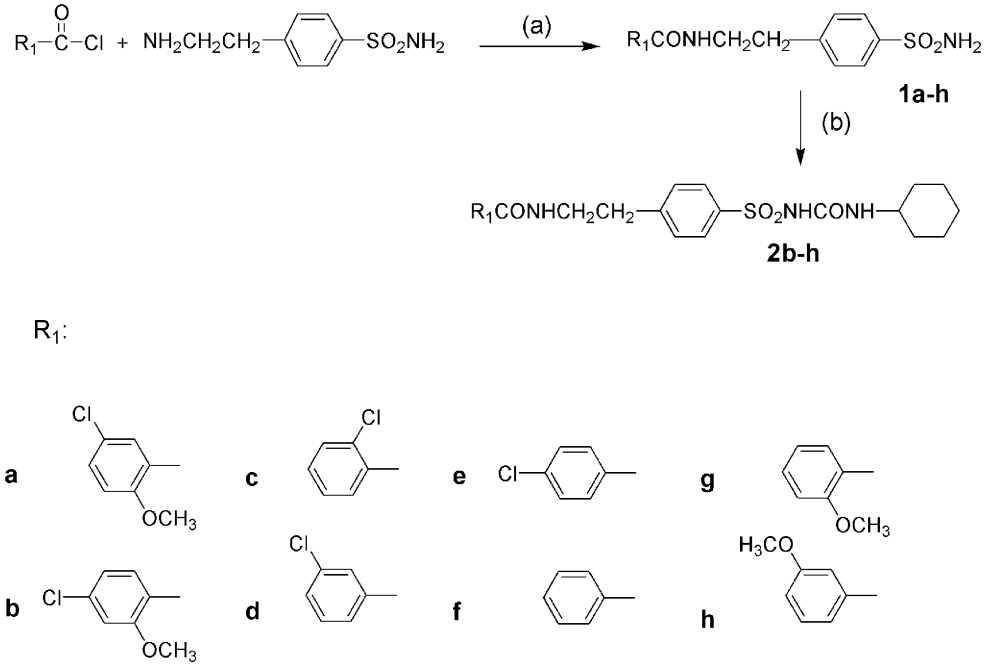

Scheme 1. Synthesis of sulfonamide and amidoethylbenzenesulfonylurea analogues. (a) Dry acetone. (b) Cyclohexylisocyanate, anhydrous potassium carbonate.

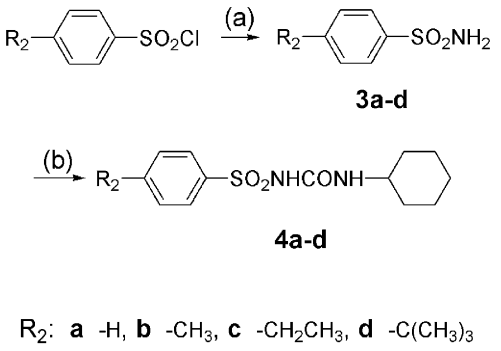

Scheme 2. Synthesis of benzenesulfonylurea analogues. (a) 25% Ammonia solution. (b) Cyclohexylisocyanate, anhydrous potassium carbonate.

three-fold aim: (i) to correlate the theoretically-observed conformational trends with those observed in the relevant experimental structures; (ii) to resolve the discrepancy between previous conformational analysis simulations [18–20], and (iii) to investigate the differences of the conformational trends in vacuo and in solvated medium.

3.1.1. Monte Carlo conformational analysis

Monte Carlo conformational analysis was carried out in vacuo and yielded the clusters of torsion values, accessible for each rotatable bond, which are best visualized as conformational wheels (Fig. 2). Additional wheels (not shown) were also generated, where frequency and strain energy of particular conformations were used to further identify the preferred conformational ranges.

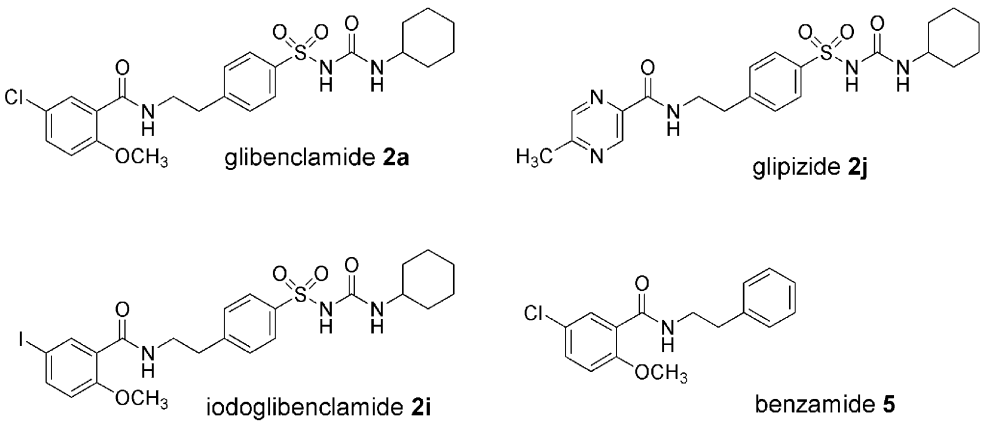

Scheme 3. Additional glibenclamide analogues used for 3D-QSAR analysis.

Table 1
pK_i values of the inhibition of [^{3}H]-glibenclamide binding in rat cerebral cortex

Compound number	pK_i
1a	6.76
2a	10.19
2b	9.64
2c	8.58
2d	9.44
2e	9.07
2f	8.66
2g	9.52
2h	9.28
2i	9.88
2j	8.86
4b	6.14
4c	6.51
4d	6.50
5	6.02

See reaction schemes for compounds' structures.

The values of the torsional angle t1 (Fig. 2) reflect rotation of the terminal phenyl ring. This rotation is of special interest in those glibenclamide analogues, in which the terminal phenyl ring is substituted, particularly in the *ortho*-position. In our conformational analyses, this substituent was commonly found in the *anti*-orientation with respect to the carbonyl. The same arrangement was observed in the crystal structure of glibenclamide [17] and was prevalent in the relevant structures obtained from the Cambridge Structural Database (CSD).

Previously, an NMR study of glibenclamide demonstrated the free rotation around the N_{amide}–C_{sp3} and C_{sp3}–C_{sp3} bonds [17]. The respective torsion angles t2 and t3 (Fig. 2), together with the angle t4 discussed below, are determinative of the relative orientation of two aromatic rings of glibenclamide. Therefore, they influence the overall shape of the molecule, affecting either an extended or a folded shape [18–20]. Our conformational searches indicated that, indeed, the rotation around the N_{amide}–C_{sp3} bond is free. With respect to the rotation around the C_{sp3}–C_{sp3} bond, the preferred torsional angle ranges for t3 were around ±60° and ±180° (Fig. 2), as expected.

The values of the torsional angle t4 (Fig. 2) reflect rotation of the middle-of-chain phenyl ring around the C_{sp3}–$C_{aromatic}$ bond. The conformational searches pointed to the near perpendicular orientation of the –CH_2–CH_2– bond with respect to the aromatic ring as preferred. Such orientation (e.g., Fig. 1, middle) leads to a partial overlap of the aromatic rings and, as a result, to the compact conformation of the benzamide part of the molecule.

The conformational environment around the sulfo group SO_2 determines the orientation of the middle-of-chain aromatic ring with respect to the cyclohexyl ring. The conformational analysis indicated the virtually unhindered rotation of this aromatic ring around the $C_{aromatic}$–S bond (torsion angle t5, Fig. 2). The rotation of the cyclohexylurea fragment around the S–N bond is represented by the torsion angle t6

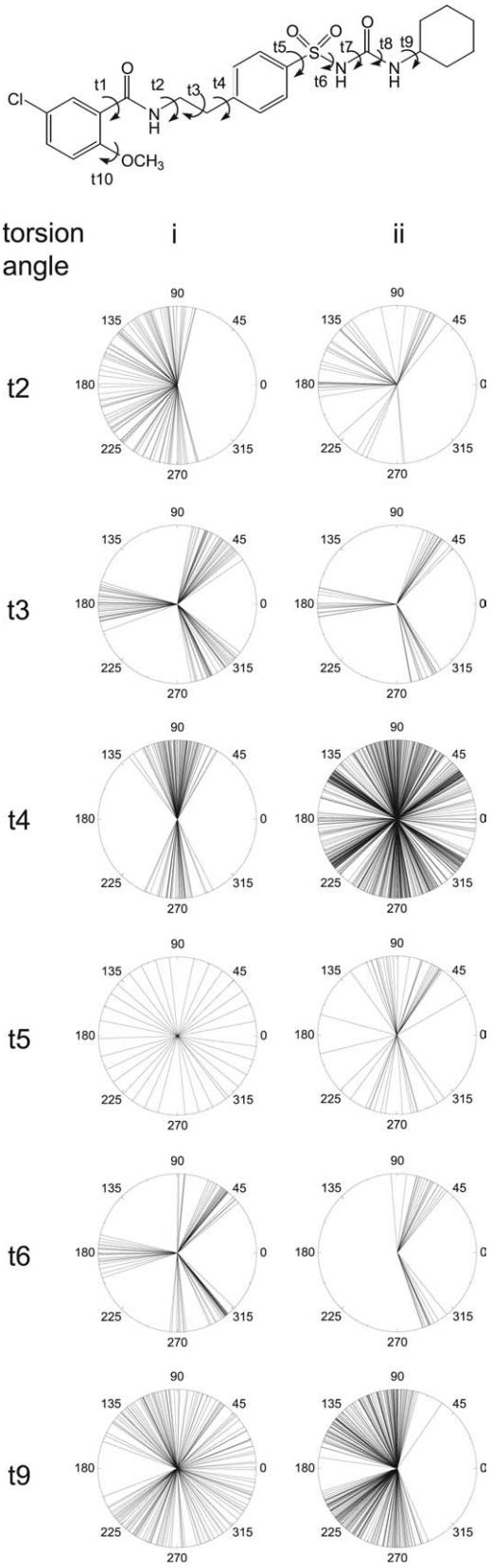

Fig. 2. Torsion angles t1–t10, varied during the conformational search, are indicated. Conformational wheels are shown for torsion angles t2–t6 and t9. Torsion angle distributions are from: (i) Monte Carlo conformational search and (ii) CSD.

(Fig. 2), which clustered around ±60° and ±180° regions (Fig. 2), with regions around ±60° being significantly favoured, both statistically and energetically.

Finally, the torsion angle t9 (Fig. 2) and the conformation of the cyclohexyl ring control the orientation of the cyclohexyl ring with respect to the urea moiety. The conformational search yielded the chair conformation of the cyclohexyl in all found structures. The rotation around the torsion angle t9 was found to be virtually free (Fig. 2), but the areas around ±120° were significantly preferred, both energetically and statistically.

The torsion angles t7, t8, and t10 (Fig. 2) were not included into the Monte Carlo conformational searches although, in principle, rotation is possible around the respective bonds. The rotation around the amide bonds of the urea moiety is controlled by the torsion angles t7 and t8 (Fig. 2). In the crystal structure of glibenclamide [17] both bonds are in the *trans* arrangement and this arrangement was found to be prevalently represented in CSD. Similarly, the analysis of the crystal structures showed that the t10 torsion angle values cluster around 180° (i.e., the methyl group is pointing away from the carbonyl). This arrangement is intuitively apparent (due to steric restrictions otherwise) and is observed in the crystal structure of glibenclamide [17].

Thus, we have accomplished the first aim (to correlate the theoretically-observed conformational trends with those detected in the relevant experimental structures) and concluded that the results of our conformational analyses agree well with the torsion angle distributions found in the relevant structures from CSD and are in accord with previous experimental structural investigations of glibenclamide [17].

3.1.2. Systematic conformational analysis

Systematic conformational analyses based on the accessible angle ranges, determined as described above, were carried out in vacuo and in explicit aqueous solution. Such simulations allow appropriate accounting for solvent effects on the energy and conformation. The conformations of the lowest energy structures obtained in vacuo and in solution are depicted in Fig. 1, middle and bottom, respectively. While similar torsion ranges were observed in vacuo and in the aqueous solution (data not shown), the overall conformations of the lowest energy structures were significantly different. The systematic conformational search carried out in vacuo favoured the highly folded conformation (Fig. 1, middle), resembling the U-shaped structure modelled by Lins et al. [18,19]. Adding the explicit solvent to the modelled environment benefited a more extended molecular shape of glibenclamide (Fig. 1, bottom), as predicted by Grell et al. [20]. While these results resolve the discrepancy between previous molecular modelling simulations of glibenclamide (second aim of the conformational analysis effort–see above), they also raise issues with respect to the effect of aqueous environment on the overall conformation. A priori, in an aqueous environment, the hydrophobic fragments of the molecule (i.e., aromatic and aliphatic rings) would prefer to be minimally exposed leading to a folded conformation. However, in this case, the groups that surround these fragments (i.e., chloro, methoxy, carbonyl, sulfo, amide) are all polarizable and are good hydrogen bonding donors/acceptors. As a result, these groups make the hydrophobic fragments more soluble and push them into the bulk solvent and away from each other, thus favouring the extended conformation. On the other hand, the folded conformation is preferred in vacuum because the effect of the polar/hydrogen bonding groups is not as pronounced as it is in aqueous solution. Furthermore, in vacuum the van der Waals interactions, especially stacking, are significant. Whereas this rationalisation accomplishes our third aim (to investigate the differences of the conformational trends in vacuo and in solvated medium–see above), it leaves open to discussion the identity of the biologically active conformation(s) of glibenclamide and the related structures and, consequently, the conformation(s) to be used 3D-QSAR analyses.

It is unarguable that the selection of bioactive conformation is the critical point in a 3D-QSAR study. Generally, albeit not always, the best choice for a bioactive conformation is the one extracted from a receptor–ligand structure. In the case of SUR–sulfonylurea interaction, the complex structure, even the structure of the isolated receptor that would lend itself to a docking approach, is not yet available. In cases such as that it is usually assumed that a ligand will adopt a bioactive conformation so as to achieve a relatively low strain energy. Thus, if a crystal structure for a ligand is available it is usually used for a 3D-QSAR analysis. An example of such application is a recent CoMSIA study on sulfonylureas [21]. However, the present case offers three options with respect to low energy conformations. Specifically, the crystal structure of glibenclamide [17]–extended conformation, the lowest energy conformation generated in vacuum–fully folded, and the lowest energy conformation generated in explicit aqueous environment and resembling that in the solid state. This choice is confounded by the great flexibility of the glibenclamide and its analogues, as demonstrated by conformational analyses presented above. It is accepted that conformational flexibility is one of the greatest challenges to selecting a ligand for CoMFA [22]. Such flexibility results in a number of diverse local conformational minima within a narrow range of energies (including the conformation of the crystal structure). We agree with Lins et al. [19] that there is probably a link between the lowest energy conformation of glibenclamide and its biological activity. However, we also support Grell et al. [20] notion that it is reasonable to consider a range of low energy conformations as favourable potential binding conformations. Furthermore, it should not be neglected that, in case of flexible molecules, binding to the receptor may modify the interaction energy resulting in a ligand conformation not revealed by a conformational search of an isolated ligand [23]. Having weighed out these arguments and our data, we decided that, out of the accessible low energy candidates, the crystal structure of glibenclamide [17] is the best available approximation for a bioactive conformation and should be used as a basis for a 3D-QSAR analysis.

3.2. CoMFA of glibenclamide analogues

CoMFA results are presented in Table 2 and demonstrated in Fig. 3. The best model (B) utilizes steric fields and Log*P* values as variables and only requires two PLS components to achieve the best statistics observed. This model predicts well the biological activity studied as demonstrated by the prediction plot (Fig. 4). However, a caveat is warranted with respect to this prediction plot: while the formal statistical measures of the quality of this model are good (Table 2), it must be pointed out that the activity data used is distributed in a bimodal fashion. The second-best model is model D, which utilizes steric and electrostatic fields and Log*P* values as variables and, again, just two PLS components are sufficient to produce good statistics. It should be commented that these models combine two different types of variables: interaction fields (which are 'multicolumn' data) and scalar Log*P* (a single data point for each compound). Although, such combinations are an extension of a traditional molecular field analysis, their use is a common tactic in the 3D-QSAR field (e.g., [24]). In addition to the variables in model B, model D accounts for electrostatic fields, however the electrostatic contribution is small (6%). Thus, both models suggest that electrostatics had very little contribution to the quantitative structure–activity relationship in this set of compounds. However, this may be not the intrinsic feature of the relationship, but rather the artefact resulting from limited structural variation in the studied compounds.

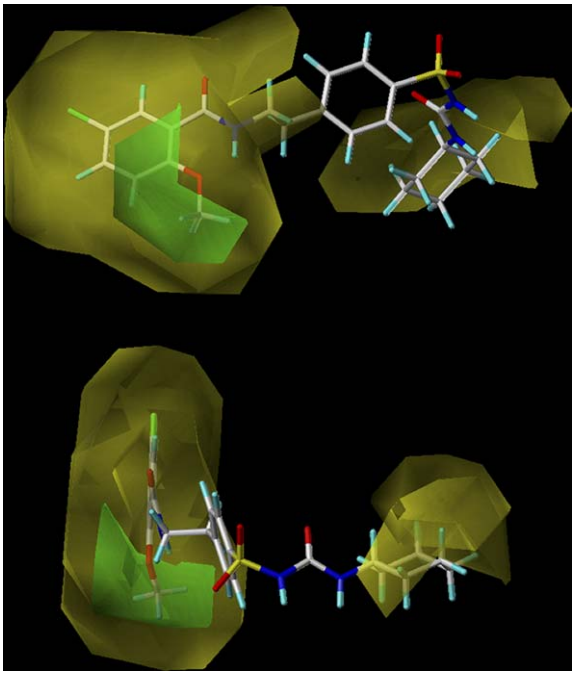

Fig. 3. Steric CoMFA map for model B showing contributions to glibenclamide activity. Yellow denotes regions where steric bulk is detrimental to activity and green denotes regions where steric bulk enhances activity (standard 80/20 settings). Two views allowing the clear observation of all features of the glibenclamide molecule are shown.

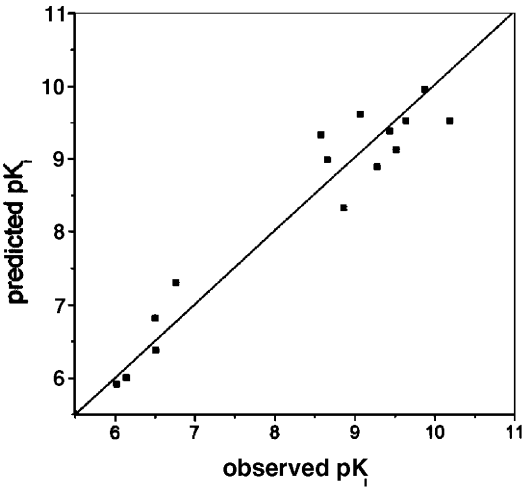

Fig. 4. Correlation of experimental vs. predicted biological activity for glibenclamide and glibenclamide analogues (amidoethylbenzenesulfonylureas **2a–j**, sulfonamide **1a**, benzenesulfonylureas **4b–d**, and benzamide **5**) using CoMFA model B. pK_i, inhibition of [^{3}H]-glibenclamide binding in rat cerebral cortex [16]. The diagonal represents the *y*=*x* line (optimal prediction).

Table 2
CoMFA models

Models	A	B	C	D
Variables [a]	Steric electro	Steric Log*P*	Electro Log*P*	Steric electro Log*P*
Statistics				
No. of components	2	2	3	2
q^2	0.623	0.876	0.850	0.829
R^2	0.909	0.921	0.924	0.895
SEP	0.994	0.569	0.655	0.669
SEE	0.488	0.455	0.466	0.524
F	60	70	44	51
Prob	0.000	0.000	0.000	0.000
Contributions				
Steric	0.722	0.447		0.319
Electro	0.278		0.525	0.060
Log*P*		0.553	0.475	0.621

[a] Variables: no. components, optimum number of components obtained from cross-validated PLS analysis; R^2, correlation coefficient; q^2, cross-validated correlation coefficient; SEP, standard error of prediction; SEE, standard error of estimate; *F*, *F*-statistic; prob, probability of the null hypothesis (both *F* and prob are tests for $R^2 = 0$ hypothesis).

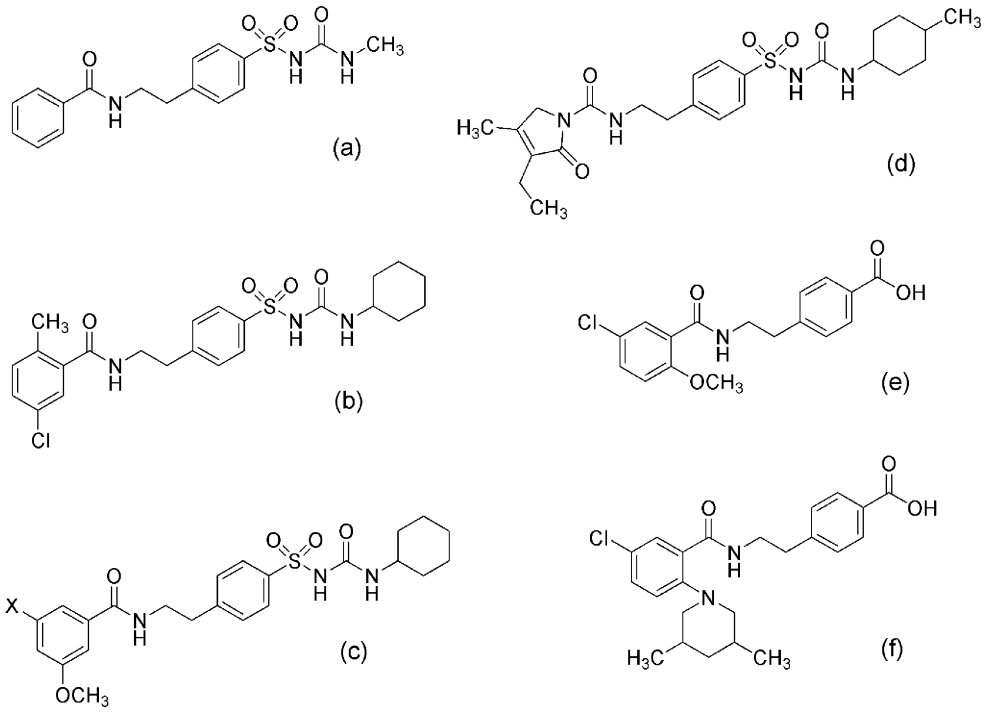

Fig. 5. Structures of glibenclamide analogues used for predictive CoMFA calculations. X, halogen.

According to the visual representation of model B (Fig. 3), steric bulk is desirable (green) around the phenyl ring of the benzamide moiety with preference for the side of the ring *anti* to the direction of the carbonyl of the amide bond; it is also more favourable in the plane of the ring, which indicates preference for halogen substituents. Steric bulk is unfavourable (yellow) 'above' the cyclohexyl ring, i.e., in the direction of the carbonyl of the urea moiety. Since in this series of analogues the structural and, hence, conformational variation is limited to the substitution of the phenyl ring and to the presence/absence of certain structural features in compounds **1a, 4b–d**, and **5**, the steric field clouds are concentrated mainly around the phenyl ring. Therefore, the design of new analogues based on this CoMFA study may be done primarily with respect to phenyl ring substitution.

3.3. CoMFA-based predictions of biological activity

Based on the CoMFA results presented above for the studied series of compounds, pK_i values were calculated for some glibenclamide derivatives (Fig. 5) using model B.

When the cyclohexyl ring in **2f** (pK_i = 8.66) was replaced with the methyl group (Fig. 5a), the resulting pK_i (7.90) decreased, suggesting the importance of the cyclohexyl ring for the observed activity. This is in agreement with other studies on structural requirements of sulfonylureas and their analogues for interactions with SUR subtypes. Specifically, Meyer et al. [25] found that exchanging the cyclohexyl ring of glibenclamide by a methyl group reduces its selectivity for SUR1. Also, it has been shown in a recent study on inhibition of [^{3}H] glibenclamide binding to rat brain synaptomes [11] that while the activity of glibenclamide analogues does not decline significantly upon hydroxylation of the cyclohexyl ring, the acyclic analogues showed markedly reduced activity compared to glibenclamide.

Since the test compounds in this CoMFA study vary mostly in the nature and the arrangement of substituents in the terminal phenyl ring of glibenclamide, the following calculations were focused on that part of the molecule. Similarly to the above, replacement of the methoxy group with methyl in the terminal phenyl ring of glibenclamide (Fig. 5b) resulted in the decreased pK_i value of 9.66, indicating the requirement for an electronegative atom at this position. This particular modification was also found to have a pronounced effect on the structural features of this derivative. Specifically, it caused the conformational change, i.e., the 180° rotation of the terminal phenyl ring. In glibenclamide, the methoxy group is in the position *anti* to benzamide carbonyl. However, the methyl group in this derivative is in the *syn* arrangement (as shown in Fig. 5). While it is obvious that such conformational adjustment is due to steric reasons (less repulsion between the carbonyl oxygen and the methyl carbon), it also indicates that the *anti* arrangement, observed in glibenclamide, is likely to be preferred for biological activity. Thus, whereas $OCH_3 \rightarrow CH_3$ modification leads to the increase in Log*P*, which could have been expected to result in the increase in pK_i, it is clearly detrimental for steric and electronic properties of the molecule.

Substitution of *meta*-hydrogen of **2h** (pK_i = 9.28) with halogens X (Fig. 5c) was studied because glibenclamide itself carries chlorine at this position. Whereas the substitution with chlorine produced virtually no effect on pK_i (9.26), the iodine at this position resulted in the increase of pK_i to 9.72, which is closer to the pK_i of iodoglibenclamide (9.88),

which carries the iodine substituent in the same position. Taken in isolation, this modification would point toward the preference for iodine at this position. However, the comparison of activities of glibenclamide and iodoglibenclamide suggests the preference for chlorine at the same location. This seeming discrepancy is resolved by the examination of the conformations of these derivatives, in particular–of the orientations of the terminal phenyl ring with respect to the carbonyl group of the amide. Specifically, as outlined above for OCH_3 *vs*. CH_3 substitution, the preferred arrangement of the *ortho*-methoxy group in glibenclamide and iodoglibenclamide is in the *anti* orientation with respect to the carbonyl due to steric reasons. This restriction places a halogen atom into a particular location in space and brings out the preference for chlorine. On the other hand, the methoxy group in **2h** is in the *meta*-position with respect to the amide bond and is not sterically restricted. This results in the relatively free rotation of the phenyl ring and in no observable preferences of the orientation of the substituents with respect to the amide bond. Thus, the comparison of glibenclamide activity to its two actual and two hypothetical derivatives shows the importance of both the nature of groups/atoms used for substitution as well as their substitution location and, in particular, the resulting conformations.

Using CoMFA model B, biological activity values (pK_i) were also calculated for some sulfonamide-related hypoglycaemic agents: glimepiride, meglitinide, and meglitinide derivative (Fig. 5d–f). The resulting pK_i values were 10.1, 6.67, and 6.76, respectively. It is impossible to absolutely verify these predictions, because the experimental pK_i of these compounds were not determined alongside the experimental pK_i values used in the current study. However, the result of pK_i = 10.1 for glimepiride indicates the good predicting ability of this model since, according to literature (for example [26,27]), this compound shows activity similar to glibenclamide. On the other hand, for the purpose of this comparison it must be born in mind that glibenclamide and glimepiride may be binding to the different receptor sites [7,28,29]. These predictions lend themselves to cautious speculations with respect to the structure–activity relationships. Specifically, the decreased pK_i values of the benzoic acid analogues indicate the importance of the sulfo group (as compared to carboxy), probably due to the altered geometry of sulfur (compared to carbon). Again, this theoretical CoMFA-based prediction is in accord with experimental findings related to the structural requirements of sulfonylureas and their analogues for interactions with SUR subtypes. Namely, Meyer et al. [25] found that the replacement of the carboxyl group of meglitinide by a sulfonylurea group significantly increased the affinities for SUR1 and SUR2. On the other hand, there is a strong opinion in the field of the anti-diabetic agents that it is the acidic/anionic function (e.g., carboxy [25] or phosphate [30]), rather than the sulfonylurea group per se of the first and second generation agents, that is essential for drug activity [3]. The more recently evolved group of compounds, styled glinides (such as meglitinide and nateglinide [31]), which are based on the non-sulfonylurea part of glibenclamide, do block K_{ATP} channels, albeit seem to interact with different regions of SUR [3].

Table 3
CoMFA-predicted diiodo analogue inhibition activities

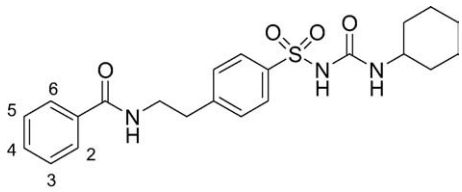

Analogue	2,4-Diiodo	2,5-Diiodo	3,5-Diiodo
Model F	10.60	10.65	10.69
Model H	10.71	10.74	10.76

Therefore, CoMFA models as well as CoMFA predictions pointed to the importance of the following structural elements for the biological activity: sulfo group, cyclohexyl, and selective substitution at the terminal phenyl ring (Fig. 2). The above analysis also produced positive indicators for halogen substitution. Specifically, such substitution allows significant Log*P* contribution to the model and agrees with the preference for steric bulk localization in the plane of the phenyl ring. Encouraged by these indicators, we carried out systematic predictive CoMFA calculations of biological activity for iodo-substituted glibenclamide analogues in the terminal phenyl ring. The predicted pK_i values for monosubstituted analogues (9.81–9.87) demonstrated that, while the position of iodo-substitution does not affect the activity, this choice of halogen, compared to chlorine (8.58–9.44) [16], significantly improves it. These values were very close to that of iodoglibenclamide, suggesting that the methoxy group in iodoglibenclamide may be irrelevant for the activity. Further encouraged by these findings, we calculated the pK_i values for diiodo substituted analogues, which are summarized in Table 3. Interesting observation was made while optimizing the analogue structures for these calculations. The 2,6-diiodo analogue was highly strung sterically and exhibited the strain energy more than 8 kcal/mol above that for all other compounds in this series. While this could be an indication of the steric repulsion between the amide carbonyl and the neighbouring iodo-substituents, it was interesting to observe that in the 2,4- and 2,5-diiodo analogues the iodine atoms, neighbouring with the carbonyl group, preferred to occupy the *syn* rather than *anti*-orientation with respect to the carbonyl oxygen. Out of three sterically and conformationally allowed diiodo substitutions (Table 3), 3,5-diiodo analogue was found to be the most energetically favoured (with the energy well of approximately 6 kcal/mol). All three compounds produced the highest predicted activity, superseding that of glibenclamide!

4. Conclusions

Molecular modelling of glibenclamide and its derivatives, presented in this work, was aimed at clarifying the structure–

activity relationships of glibenclamide analogues in quantitative terms using conformational analysis and CoMFA study of these compounds. The detailed conformational analysis in vacuum and in explicit aqueous solution provided data complementary to previously published NMR and X-ray investigations of glibenclamide. It also allowed us critically revisiting the conclusions of earlier reported conformational study of glibenclamide done purely in vacuum. CoMFA models as well as CoMFA predictions for modified analogues confirmed the importance of several structural elements for the K_{ATP} channel blocking activity and allowed arriving at a set of rules for the design of new compounds with improved activity–rules to be used at the bench in order to improve new pharmacomodulations. It must be noted that the studied series of compounds is limited and this study focused on developing a robust model and not in investigating its predictive power with an external and large test set.

5. Experimental

5.1. Chemistry

Melting points were determined on Gallenkamp MFB-595 apparatus and are uncorrected. Infra-red spectra were recorded using a Hitachi 270-30 grating spectrophotometer as potassium bromide discs. Positive ion Fast Atom Bombardment (FAB) mass spectra were obtained on a Joel JMX DX-300 double focussing instrument. Incident particle used was Xenon. Microanalysis was conducted by the National Analytical Laboratory Ltd and had an error of ±0.4%. ^{1}H NMR data were recorded using a Bruker AM-300 MHz instrument. Chemical shifts were expressed in parts per million (ppm) using tetramethylsilane (TMS) as the standard reference. All spectra were recorded in 5 mm tubes. Analytical thin-layer chromatography (TLC) was performed on Merck Kieselgel 60 F_{254} precoated aluminium backed plates. Column chromatography was performed either on Merck Kieselgel 60 (70–230 mesh ASTM) silica or Merck Kieselgel 60 (230–400 mesh ASTM) silica. All chemicals used were reagent grade and were distilled, recrystallized or dried with molecular sieves prior to use. For synthesis of related compounds which follows the same procedure, a general procedure has been outlined for one compound. All compounds following the same procedure have been indicated and any variations from the general procedure are mentioned. Unless otherwise stated, all compounds used were purchased from Aldrich.

5.1.1. General procedure for the synthesis of 4-(2-(benzamido)ethyl)benzenesulphonamides (**1a–c, 1h**)

Appropriate benzoyl chloride was added slowly to a stirred solution of 4-(2-aminoethyl)benzenesulphonamide in dry pyridine (60 ml). The resultant mixture was stirred for 16 h. Pyridine was removed under reduced pressure and absolute ethanol (40 ml) was added to the residue. The crude compound was filtered and recrystallized from methanol and decolourising charcoal to give white plates.

*5.1.1.1.4-(2-(5-Chloro-2-methoxybenzamido)ethyl)benzenesulphonamide (**1a**).* Compound **1a** was synthesized from 5-chloro-2-methoxybenzoyl chloride (2.05 g, 10 mmol) and 4-(2-aminoethyl)benzenesulphonamide (2.00 g, 10 mmol). Yield, 1.89 g (59.8%); mp: 213–215 °C (lit. mp: 214–216 °C, [32]); TLC R_f 0.74, 8:2 chloroform/methanol. *m/z* (relative intensity) 368 ($M^{+\cdot}$ +1, 86%), 169 (100%). Accurate mass 369.06758 requires C16 H18 N2 O4 S1 Cl1. ν_{max} 3380, 3292, 1616, 1544, 1340, 1158, 682 cm^{-1}.

*5.1.1.2.4-(2-(4-Chloro-2-methoxybenzamido)ethyl)benzenesulphonamide (**1b**).* Compound **1b** was synthesized from 4-chloro-2-methoxybenzoyl chloride (4.10 g, 20 mmol) and 4-(2-aminoethyl)benzenesulphonamide (4.00 g, 20 mmol). Yield, 4.36 g (59.2%); mp: 186–187 °C (lit. mp: 187–188 °C, [32]); TLC R_f 0.73, 8:2 chloroform/methanol. *m/z* (relative intensity) 368 ($M^{+\cdot}$ +1, 60%), 169 (80%). ν_{max} 3388, 3334, 1626, 1530, 1332, 1239, 1152, 642 cm^{-1}.

*5.1.1.3. 4-(2-(2-Chlorobenzamido)ethyl)benzenesulphonamide (**1c**).* Compound **1c** was synthesized and from 2-chlorobenzoyl chloride (2.70 g, 15.4 mmol) and 4-(2-aminoethyl)benzenesulphonamide (3.10 g, 15.4 mmol). Yield, 3.58 g (70.6%); mp: 198–199 °C (lit. mp: 195–196 °C, [33]); TLC R_f 0.87, 8:2 chloroform/methanol. *m/z* (relative intensity) 339 ($M^{+\cdot}$ +1, 63%), 139 (100%). ν_{max} 3370, 3292, 1629, 1548, 1317, 1290, 1152, 660 cm^{-1}.

*5.1.1.4. 4-(2-(3-Methoxybenzamido)ethyl)benzenesulphonamide (**1h**).* Compound **1h** was synthesized from 3-methoxybenzoyl chloride (1.71 g, 10 mmol) and 4-(2-aminoethyl)benzenesulphonamide (2.00 g, 10 mmol). Yield, 2.02 g (60.5%); mp: 163–164 °C (lit. mp: 162 °C, [33]); TLC R_f 0.84, 8:2 chloroform/methanol. *m/z* (relative intensity) 335 ($M^{+\cdot}$ +1, 100%), 135 (100%). Accurate mass 335.10395 requires C16, H19, N2, O4, S1. ν_{max} 3334, 3280, 1629, 1536, 1317, 1236 1155, 684 cm^{-1}.

5.1.2. General procedure for the synthesis of 4-(2-(benzamido)ethyl)benzenesulphonamides (**1d–g**)

Appropriate benzoyl chloride was added slowly to a stirred solution of 4-(2-aminoethyl)benzenesulphonamide in dry pyridine (60 ml). The resultant mixture was stirred for 16 h. After the removal of pyridine under vacuum, a viscous yellow liquid was obtained. When this viscous residue was treated with hydrochloric acid (1 M, 50 ml), a yellowish solid was formed. This was filtered, washed with water and recrystallized as white needles from absolute ethanol.

*5.1.2.1. 4-(2-(3-Chlorobenzamido)ethyl)benzenesulphonamide (**1d**).* Compound **1d** was synthesized from 3-chlorobenzoyl chloride (3.48 g, 20 mmol) and 4-(2-aminoethyl)-benzenesulphonamide (4.00 g, 20 mmol). Yield, 2.14 g

(31.7%); mp: 161–163 °C (lit. mp: 161–163 °C, [32]); TLC R_f 0.81, 8:2 chloroform/methanol. *m/z* (relative intensity) 339 ($M^{+\cdot}$ +1, 52%), 139 (100%). ν_{max} 3328, 1626, 1533, 1332, 1152 cm^{-1}.

*5.1.2.2. 4-(2-(4-Chlorobenzamido)ethyl)benzenesulphonamide (**1e**).* Compound **1e** was synthesized from 4-chlorobenzoyl chloride (3.48 g, 20 mmol) and 4-(2-aminoethyl)benzenesulphonamide (4.00 g, 20 mmol). Yield, 3.46 g (51.2%); mp: 222–223 °C (lit. mp: 225–226 °C, [32]); TLC R_f 0.86, 8:2 chloroform/methanol. *m/z* (relative intensity) 339 ($M^{+\cdot}$ +1, 36%), 139 (71%). Accurate mass 339.05915 requires C15, H16, N2, O3, S1, Cl1. ν_{max} 3400, 3328, 1632, 1542, 1323, 1155, cm^{-1}.

*5.1.2.3. 4-(2-(Benzamido)ethyl)benzenesulphonamide (**1f**).* Compound **1f** was synthesized from benzoyl chloride (1.41 g, 10 mmol) and 4-(2-aminoethyl)benzenesulphonamide (2.00 g, 10 mmol). Yield, 1.70 g (56.0%); mp: 249–250 °C; TLC R_f 0.81, 8:2 chloroform/methanol. *m/z* (relative intensity) 305 ($M^{+\cdot}$ +1, 43%), 105 (29%). Accurate mass 305.09385 requires C15, H17, N2, O3, S1. Microanalysis expected values C 59.2%, H 5.3%, N 9.2% and S 10.5%. Found C 59.2%, H 5.6%, N 9.3%, and S 10.5%. ν_{max} 3388, 3190, 1617, 1542, 1326, 1149, 684 cm^{-1}.

*5.1.2.4. 4-(2-(2-Methoxybenzamido)ethyl)benzenesulphonamide (**1g**).* Compound **1g** was synthesized from 2-methoxybenzoyl chloride (1.71 g, 10 mmol) and 4-(2-aminoethyl)benzenesulphonamide (2.00 g, 10 mmol). Yield, 1.25g (37.4%); mp: 177–179 °C (lit. mp: 173–174 °C, [33]); TLC R_f 0.84, 8:2 chloroform/methanol. *m/z* (relative intensity) 335 ($M^{+\cdot}$ +1, 38%), 135 (100%). Accurate mass 335.10689 requires C16, H19, N2, O4, S1. ν_{max} 3352, 3184, 1623, 1539, 1323, 1239 1155, 696 cm^{-1}.

*5.1.3. General procedure for the synthesis of 4-(2-(benzamido)ethyl)benzenesulfonyl-3-cyclohexylureas (**2b, 2e–h**)*

Appropriate 4-(2-(benzamido)ethyl)benzenesulphonamide was refluxed in a stirred solution of anhydrous potassium carbonate (415 mg, 3 mmol) in acetone (25 ml) for 1.5 h under dry conditions. At that temperature, cyclohexylisocyanate (200 mg, 1.6 mmol) in dry acetone (4 ml) was added dropwise. The resultant mixture was refluxed for another 16 h. Acetone was removed under vacuum and water (30 ml) was added to the white residue. The mixture was acidified with concentrated hydrochloric acid to pH 1. White precipitate was filtered and recrystallized from methanol.

*5.1.3.1. 1-(4-(2-(4-Chloro-2-methoxybenzamido)ethyl)benzenesulfonyl)-3-cyclohexylurea (**2b**).* Compound **2b** was synthesized from **1b** (368 mg, 1 mmol), anhydrous potassium carbonate (415 mg, 3 mmol) and cyclohexylisocyanate (200 mg, 1.6 mmol). Yield, 309 mg (62.2%) of white rods; mp: 197–199 °C (lit. mp: 200–201 °C, [34]); TLC R_f 0.59, 95:5 chloroform/methanol. *m/z* (relative intensity) 494 ($M^{+\cdot}$ +1, 5%), 369 (23%), 169 (100%). Accurate mass 494.15232 requires C23, H29, N3, O5, C11, S1. Micro analysis expected values C 55.9%, H 5.7%, N 8.5%, and S 6.5%. Found C 55.5%, H 5.9%, N 8.6%, and S 6.5%. ν_{max} 3364, 2932, 1623, 1593, 1527, 1449, 1248, 1155 cm^{-1}.

*5.1.3.2. 1-(4-(2-(4-Chlorobenzamido)ethyl)benzenesulphonyl)-3-cyclohexylurea (**2e**).* Compound **2e** was synthesized from **1e** (676 mg, 2 mmol), anhydrous potassium carbonate (830 mg, 6 mmol) and cyclohexylisocyanate (400 mg, 3.2 mmol). Yield, 564 mg (60.9%) of white needles; mp: 197–199 °C (lit. mp: 196–197.5 °C, [33]); TLC R_f 0.62, 9.5:0.5 chloroform/methanol. *m/z* (relative intensity) 464 ($M^{+\cdot}$ +1, 2%), 339 (29%), 139 (100%). ν_{max} 3384, 2932, 1634, 1532, 1442, 1232, 1154 cm^{-1}.

*5.1.3.3. 1-(4-(2-(Benzamido)ethyl)benzenesulphonyl)-3-cyclohexylurea (**2f**).* Compound **2f** was synthesized from **1f** (608 mg, 2 mmol), anhydrous potassium carbonate (830 mg, 6 mmol) and cyclohexylisocyanate (400 mg, 3.2 mmol). Yield, 72 mg (8.34%) of white needles; mp: 187–189 °C (lit. mp: 189–191 °C, [33]); TLC R_f 0.38, 9.5:0.5 chloroform/methanol. *m/z* (relative intensity) 430 ($M^{+\cdot}$ +1, 7%), 305 (100%). Accurate mass 430.17894 requires C22 H28 N3 O4 S1. ν_{max} 3340, 2932, 1632, 1512, 1440, 1215, 1158 cm^{-1}.

*5.1.3.4. 1-(4-(2-(2-Methoxybenzamido)ethyl)benzenesulphonyl)-3-cyclohexylurea (**2g**).* Compound **2g** was synthesized from **1g** (334 mg, 1 mmol), anhydrous potassium carbonate (415 mg, 3 mmol) and cyclohexylisocyanate (200 mg, 1.6 mmol). Yield, 138 mg (30.1%) of white rods; mp: 180–182 °C (lit. mp: 184 °C, [33]); TLC R_f 0.57, 9.5:0.5 chloroform/methanol. *m/z* (relative intensity) 460 ($M^{+\cdot}$ +1, 8%), 335 (100%), 135 (100%). ν_{max} 3346, 2932, 1614, 1527, 1452, 1245, 1155 cm^{-1}.

*5.1.3.5. 1-(4-(2-(3-Methoxybenzamido)ethyl)benzenesulphonyl)-3-cyclohexylurea (**2h**).* Compound **2h** was synthesized from **1h** (334 mg, 1 mmol), anhydrous potassium carbonate (415 mg, 3 mmol) and cyclohexylisocyanate (200 mg, 1.6 mmol). Yield, 122 mg (26.6%) of white rods; mp: 181–182 °C (lit. mp: 184-185°C, [33]); TLC R_f 0.65, 95:5 chloroform/methanol. *m/z* (relative intensity) 460 (M^{+} ·+1, 4%), 335 (60%), 135 (100%). ν_{max} 3322, 2932, 1623, 1584, 1521, 1446, 1245, 1155, 1026 cm^{-1}.

*5.1.4. 1-(4-(2-(2-Chlorobenzamido)ethyl)benzenesulphonyl)-3-cyclohexylurea (**2c**)*

Compound **2c** was prepared by refluxing **1c** in a stirred solution of anhydrous potassium carbonate (415 mg, 3 mmol) in acetone (25 ml) for 1.5 h under dry conditions. At that temperature, cyclohexylisocyanate (200 mg, 1.6 mmol) in dry acetone (4 ml) was added dropwise. The resultant mixture was refluxed for another 16 h. On removal of acetone under vacuum, 1 M sodium hydroxide (50 ml) was added. The reaction mixture was filtered and then acidified with

concentrated hydrochloric acid to pH 1. The resultant precipitate was filtered and recrystallized from methanol. Yield, 80 mg (8.6%) of white needles; mp: 202–204 °C (lit. mp: 204–205 °C, [33]); TLC R_f 0.58, 9.5:0.5 chloroform/methanol. *m/z* (relative intensity) 464 ($M^{+\cdot}$ +1, 5%), 339 (46%), 139 (100%). ν_{max} 3358, 2932, 1635, 1593, 1527, 1449, 1221, 1155 cm^{-1}.

*5.1.5. 1-(4-(2-(3-Chlorobenzamido)ethyl)benzenesulphonyl)-3-cyclohexylurea (**2d**)*

Compound **2d** was synthesized from **1d** (676 mg, 2 mmol), anhydrous potassium carbonate (830 mg, 6 mmol) and cyclohexylisocyanate (400 mg, 3.2 mmol). After refluxing the reaction mixture for 16 h, acetone was removed under reduced pressure and then 1 M HCl (50 ml) was added. The white precipitate was filtered and recrystallized twice from methanol. Yield, 374 mg (40.4%) of white needles; mp: 191–192 °C (lit. mp: 190–191 °C, [34]); TLC R_f 0.60, 9.5:0.5 chloroform/methanol. *m/z* (relative intensity) 464 ($M^{+\cdot}$ +1, 2%), 339 (29%), 139 (100%). ν_{max} 3384, 2930, 1634, 1528, 1445, 1224, 1154 cm^{-1}.

*5.1.6. General procedure for the synthesis of benzenesulphonamides (**3a–d**)*

Appropriate benzenesulphonyl chloride was added dropwise to a stirred 25% ammonia solution (45 ml). The resultant mixture was heated to 100 °C and cooled to room temperature. The product was recrystallized from water.

*5.1.6.1. Benzenesulphonamide (**3a**).* Compound **3a** was synthesized from benzenesulphonyl chloride (9.2 g, 0.052 mole). Yield, 4.62 g (56.6%) of white plates; mp: 146–147 °C (lit. mp: 147–148 °C, [35]); TLC R_f 0.48, 9:1 chloroform/methanol. *m/z* (relative intensity) 158 ($M^{+\cdot}$ +1, 100%), 141 (33%). ν_{max} 3370, 3274, 1335, 1155 cm^{-1}.

*5.1.6.2. 4-Methylbenzenesulphonamide (**3b**).* Compound **3b** was synthesized from 4-methylbenzenesulphonyl chloride (10.0 g, 0.052 mole). Yield, 7.83 g (88.1%) of colourless rods; mp: 136–137 °C (lit. mp: 138 °C, [36]); TLC R_f 0.5, 9:1 chloroform/methanol. *m/z* (relative intensity) 172 ($M^{+\cdot}$ +1, 100%), 154 (57%). ν_{max} 3328, 3244, 3132, 1322, 1146, 1086 cm^{-1}.

*5.1.6.3. 4-Ethylbenzenesulphonamide (**3c**).* Compound **3c** was synthesized from 4-ethylbenzenesulphonyl. The crude product was recrystallized from water/methanol. Yield, 0.93 g (9.5%) of white plates; mp: 103–105 °C (lit. mp: 104–107.5 °C, [37]); TLC R_f 0.51, 9:1 chloroform/methanol. *m/z* (relative intensity) 186 ($M^{+\cdot}$ +1, 86%), 169 (64%), 105 (100%). ν_{max} 3344, 3268, 1326, 1290, 1173 cm^{-1}.

*5.1.6.4. 4-*ter*-Butylbenzenesulphonamide (**3d**).* Compound **3d** was synthesized from 4-*ter*-butylbenzenesulphonyl chloride (3.0 g, 13 mmol) in dry acetone (12 ml) and 25% ammonia solution (30 ml). The crude compound was recrystallized from water/methanol and decolourising charcoal was used. Yield, 1.18 g (43.0%) of white rods; mp: 133–134 °C; TLC R_f 0.18, chloroform. *m/z* (relative intensity) 214 ($M^{+\cdot}$ +1, 100%), 197 (53%), 133 (36%). ν_{max} 3384, 3284, 1328, 1164 cm^{-1}.

*5.1.7. General procedure for the synthesis of benzenesulphonyl-3-cyclohexylureas (**4a–d**)*

Benzenesulphonyl-3-cyclohexylureas (**4a–d**) were prepared from appropriate benzenesulphonamides (**3a–d**), anhydrous potassium carbonate and cyclohexylisocyanate according to the methods described for **2b** and **2c**.

*5.1.7.1. 1-Benzenesulphonyl-3-cyclohexylurea (**4a**).* Compound **4a** was prepared from **3a** (471 mg, 3 mmol), anhydrous potassium carbonate (1.242 g, 9 mmol) and cyclohexylisocyanate (600 mg, 4.8 mmol) according to the methods described for **2c**. Yield, 378 mg (44.7%) of white rods; mp: 187–189 °C (lit. mp: 188–189 °C, [38]); TLC R_f 0.47, chloroform. *m/z* (relative intensity) 283 ($M^{+\cdot}$ +1, 100%), 200 (43%), 158 (36%), 143 (90%), 141 (51%). ν_{max} 3364, 3080, 2944, 1656, 1544, 1444, 1338, 1162 cm^{-1}.

*5.1.7.2. 1-(4-Methylbenzenesulphonyl)-3-cyclohexylurea (**4b**).* Compound **4b** was prepared from **3b** (513 mg, 3 mmol), anhydrous potassium carbonate (1.242 g, 9 mmol) and cyclohexylisocyanate (600 mg, 4.8 mmol). After the removal of acetone under vacuum, 2 M sodium hydroxide solution (50 ml) and methanol (20 ml) were added. Yield, 414 mg (46.6%) of white rods; mp: 170–172 °C (lit. mp: 171–173 °C, [38]); TLC R_f 0.46, 9.5:0.5 chloroform/methanol. *m/z* (relative intensity) 297 ($M^{+\cdot}$ +1, 84%), 215 (46%), 172 (49%), 155 (100%). ν_{max} 3328, 3172, 2932, 1641, 1527, 1446, 1338, 1155, 1029 cm^{-1}.

*5.1.7.3. 1-(4-Ethylbenzenesulphonyl)-3-cyclohexylurea (**4c**).* Compound **4c** was prepared from **3c** (555 mg, 3 mmol), anhydrous potassium carbonate (1.242 g, 9 mmol) and cyclohexylisocyanate (600 mg, 4.8 mmol). Yield, 278 mg (29.9%) of white rods; mp: 159–161 °C; TLC R_f 0.51, chloroform. *m/z* (relative intensity) 311 ($M^{+\cdot}$ +1, 47%), 229 (29%), 186 (8%), 169 (41%), 143 (36%), 105 (100%). Micro analysis expected values C 58.0%, H 7.1%, N 9.0% and S 10.3%. Found C 57.6%, H 7.3%, N 9.2% and S 10.4%. ν_{max} 3316, 3228, 2920, 1676, 1522, 1444, 1330, 1158 cm^{-1}.

*5.1.7.4. 1-(4-*ter*-Butylbenzenesulphonyl)-3-cyclohexylurea (**4d**).* Compound **4d** was synthesized and purified from **3d** (639 mg, 3 mmol), anhydrous potassium carbonate (1.242 g, 9 mmol) and cyclohexylisocyanate (600 mg, 4.8 mmol). Yield, 44 mg (6.1%) of white rods; mp: 210–211 °C; TLC R_f 0.53, chloroform. *m/z* (relative intensity) 239 ($M^{+\cdot}$ +1, 100%), 256 (33%), 214 (31%), 197 (54%), 143 (40%), 133 (86%). Accurate mass 339.17461 requires C17 H27 N2 O3 S1. Micro analysis expected values C 60.3%, H 7.7%, N 8.3% and S 9.5%. Found C 60.0%, H 7.9%, N 8.4% and S

9.6%. ν_{max} 3364, 3096, 2944, 1534, 1464, 1342, 1164, 1034 cm^{-1}.

5.1.8. N-*(2-Phenylethyl)-5-chloro-2-methoxybenzamide (**5**)*

Compound **5** was synthesized by adding 5-chloro-2-methoxybenzoyl chloride (4.10 g, 20 mmol) slowly to a stirred solution of 2-phenylethylamine (2.42 g, 20 mmol) in chloroform (20 ml) at 0 °C. The reaction mixture was filtered, washed three times with 1 M HCl solution and the organic layer dried with anhydrous sodium sulphate. Chloroform was then removed under reduced pressure to give a viscous yellow oil. This was triturated with hexane and the precipitate obtained was recrystallized from diethyl ether. Yield, 0.28 g (9.7%) of colourless plates; mp: 61–63 °C (lit. mp: 61–64 °C [39]); TLC R_f 0.91, 8:2 chloroform/methanol. *m/z* (relative intensity) 290 ($M^{+\cdot}$ +1, 100%), 169 (100%), 105 (100%). ν_{max} 3310, 2950, 1626, 1482, 1263 cm^{-1}.

5.2. Computational procedures

5.2.1. Molecular mechanics protocol

All modelling studies were carried out using HyperChem modelling package (version 5.11). Molecular mechanics energy minimizations were done using the MM+ force field of HyperChem, an extension of Allinger's MM2 force field [40]. The missing force field parameters, associated with glibenclamide and its analogues, were retrieved from literature or generated based on the structural information available from Cambridge Structural Database (for bond lengths and angles) and following the standard procedures [41] (for force constants). These are summarized in Table 4. Input molecular systems were either taken from crystal structures (where available from CSD) or model-built by modifying the crystal structures of related molecular systems. Prior to conformational searching, molecular systems were initially energy minimized to remove residual strain and bad contacts resulting from modified experimental structures and model building.

Table 4
MM+ parameters for the geometry optimisation of glibenclamide and its analogues

Bond	r_0 (Å)	K_r (mdyn/Å)	
CA–S4	1.750[a]	4.0 [42]	
C3–S2	1.700[a]	10.0[b]	
Angle	**θ_0 (degree)**	**K_θ (mdyn × Å/rad^2)**	
CA–CA–S4	120.0 [a] [43]	0.420 [43]	
CA–S4–N2	104.0 [a] [44]	1.440 [44]	
CA–S4–O1	107.7 [a] [43]	0.597 [43]	
S4–N2–CO	120.00 [a] [41]	0.695 [b]	
Torsional angle [b]	**V_1 (kcal/mol)**	**V_2 (kcal/mol)**	**V_3 (kcal/mol)**
CA–CA–CA–S4	0.000	6.250	0.000
CA–CA–S4–N2	0.000	0.033	0.000
CA–CA–S4–O1	0.000	0.033	0.000
CA–S4–N2–CO	0.000	0.033	0.000
CA–S4–N2–HV	0.000	0.033	0.000
O1–S4–N2–CO	0.000	0.033	0.000
H–CA–CA–S4	0.000	6.250	0.000
S4–N2–CO–N2	0.000	1.250	0.000
S4–N2–CO–O1	0.000	1.250	0.000
HV–N2–CO–CA	0.000	1.250	0.000
CO–CA–CA–O2	0.000	6.250	0.000
CO–N2–CO–CA	0.000	1.250	0.000
N2–CO–C3–NA	0.000	1.250	0.000
CO–C3–C3–NA	0.000	11.25	0.000
CO–C3–NA–C3	0.000	2.500	0.000
CO–C3–N2–HV	0.000	1.250	0.000
NA–C3–CO–O1	0.000	1.250	0.000

[a] Based on the statistical analysis of the CSD data.
[b] HyperChem default scheme for generating unknown parameters.

5.2.2. Geometry optimization

The molecular structures were optimized using the conjugate gradient algorithm (Polak-Ribiere) with the termination condition being RMS gradient less than 0.1 kcal/(Å × mol) (in vacuo) and 0.5 kcal/(Å × mol) (in explicit solvent (H_2O)). No cut-offs were used in vacuo, in explicit solvent the switched cut-off was used with inner and outer radii of 8.5 and 12 Å, respectively. Electrostatic interactions were modelled using the bond dipoles. For the explicit solvent calculations, the cubic periodic box with the side of 25 Å was used.

5.2.3. Monte Carlo conformational analysis

Conformational analysis was carried out at the molecular mechanics level of theory using the Conformational Search module of ChemPlus (version 1.6) with the following search options: torsion angles t1–t10 (Fig. 2); ranges for variation: 1 to 8 simultaneous variations; acyclic variation: ±60° to ±180°; torsion flexing: ±30° to ±120°; search method: usage directed; acceptance energy criterion: 6 kcal/mol above best conformation. The newly generated conformations were excluded on the pre-optimization stage if atoms were closer than 0.5 Å and if torsions were within 15° of an already accepted conformation. The geometry optimized conformations were considered duplicates of an already accepted conformation if exhibiting the torsions within 10°–15° of already accepted conformation.

5.2.4. Analysis of conformational preferences in experimental structures

Analysis of conformational preferences in experimental structures was carried out by searching CSD for structures containing relevant fragments with torsion angles of interest. The database output files were examined visually to remove the outliers and then subjected to GSTAT for a statistical analysis. GSTAT is a multi-functional geometry program within the CSD, which can perform geometrical calculations for complete CSD entries and for substructural fragments and carry out statistical and numerical analyses of fragment geometry.

5.2.5. Comparative molecular field analysis

Comparative molecular field analysis was carried out with the CoMFA unit of the molecular modelling suite of programs Sybyl (version 6.2). Input structures were based on the crystal structure of glibenclamide [17] and were modelled as described above. Gasteiger-Marsili charges were assigned for CoMFA runs. Two different positioning (database and rigid field fit) were performed, the former yielding a better alignment. In this approach, all the compounds were aligned by atom-by-atom fitting using the heavy atoms of the terminal phenyl ring and the carbon atom of the carbonyl group of the benzamide substructure. Cross-validated CoMFA runs were performed by means of PLS (leave one out) regression analysis in order to obtain the optimal number of principal components to be used in the subsequent analyses (the optimum number of components obtained from cross-validated PLS analysis and q^2–the cross-validated correlation coefficient are shown in Table 2). The number of principal components thus determined was used in the non-cross-validated CoMFA runs so as to obtain the highest correlation coefficient R^2 and the lowest standard error (Table 2). The pK_i of the inhibition of [^{3}H]-glibenclamide binding in rat cerebral cortex [16] was used as the biological activity indicator (Table 1). CoMFA was carried out with the default settings except for 2.0 kcal/mol column filtering applied at cross-validation and no-validation runs. CoMFA variable used: S, steric fields; E, electrostatic fields; P, octanol-water partition coefficient (Log*P*), calculated with ChemPlus.

Acknowledgements

This work was supported in part by The Australian Postgraduate Awards (APA) and Monash Graduate Scholarship (MGS) to DCMK.

References

[1] M.J. Coghlan, W.A. Carroll, M. Gopalakrishnan, J. Med. Chem. 44 (2001) 1627–1653.
[2] M.L.J. Ashford, in: N.S. Cook (Ed.), Potassium Channels: Structure, Classification, Function and Therapeutic Potential, Ellis Horwood, Chichester, 1990, pp. 300–325.
[3] F.M. Gribble, F. Reimann, Diabetologia 46 (2003) 875–891.
[4] V. Kecskemeti, Z. Bagi, P. Pacher, I. Posa, E. Kocsis, M.Z. Koltai, Curr. Med. Chem. 9 (2002) 53–71.
[5] M.V. Mikhailov, E.A. Mikhailova, S.J. Ashcroft, FEBS Lett. 499 (2001) 154–160.
[6] L. Luzi, G. Pozza, Acta Diabetol. 34 (1997) 239–244.
[7] W. Kramer, G. Muller, F. Girbig, U. Gutjahr, S. Kowalewski, D. Hartz, H.D. Summ, Diabetes Res. Clin. Pract. 28 (Suppl) (1995) S67–S80.
[8] C.E. Schotborgh, A.A. Wilde, Cardiovasc. Res. 34 (1997) 73–80.
[9] A.A. Konstas, M. Dabrowski, C. Korbmacher, S.J. Tucker, J. Biol. Chem. 277 (2002) 21346–21351.
[10] S. Bavirti, J.A. Tayek, Metabolism 52 (2003) 407–412.
[11] R.A. Hill, S. Rudra, B. Peng, D.S. Roane, J.K. Bounds, Y. Zhang, A. Adloo, T. Lu, Bioorg. Med. Chem. 11 (2003) 2099–2113.
[12] R. Rosskamp, K. Wernicke-Panten, E. Draeger, Diabetes Res. Clin. Pract. 31 (Suppl) (1996) S33–S42.
[13] UK Prospective Diabetes Study Group, Lancet 352 (1998) 837–853.
[14] M.C. Riddle, J. Clin. Endocrinol. Metab. 88 (2003) 528–530.
[15] P.A. Brady, A. Jovanovic, J. Am. Coll. Cardiol. 42 (2003) 1022–1025.
[16] J.L. Challinor-Rogers, D.C. Kong, M.N. Iskander, G.A. McPherson, J. Pharmacol. Exp. Ther. 273 (1995) 778–786.
[17] S.R. Byrn, A.T. McKenzie, M.M. Hassan, A.A. Al-Badr, J. Pharm. Sci. 75 (1986) 596–600.
[18] L. Lins, R. Brasseur, W.J. Malaisse, Pharmacol. Res. 34 (1996) 9–10.
[19] L. Lins, R. Brasseur, W.J. Malaisse, Biochem. Pharmacol. 50 (1995) 1879–1884.
[20] W. Grell, R. Hurnaus, G. Griss, R. Sauter, E. Rupprecht, M. Mark, P. Luger, H. Nar, H. Wittneben, P. Muller, J. Med. Chem. 41 (1998) 5219–5246.
[21] T.J. Hou, Z.M. Li, Z. Li, J. Liu, X.J. Xu, J. Chem. Inf. Comput. Sci. 40 (2000) 1002–1009.
[22] G. Klebe, U. Abraham, J. Med. Chem. 36 (1993) 70–80.
[23] H. Lanig, W. Utz, P. Gmeiner, J. Med. Chem. 44 (2001) 1151–1157.
[24] A.K. Chakraborti, R. Thilagavathi, Bioorg. Med. Chem. 11 (2003) 3989–3996.
[25] M. Meyer, F. Chudziak, C. Schwanstecher, M. Schwanstecher, U. Panten, Br. J. Pharmacol. 128 (1999) 27–34.
[26] S.A. Raptis, E. Hatziagelaki, G. Dimitriadis, K.E. Draeger, C. Pfeiffer, A.E. Raptis, Exp. Clin. Endocrinol. Diabetes 107 (1999) 350–355.
[27] Prescrire Int. 7 (1998) 106–107.
[28] W. Kramer, G. Muller, F. Girbig, U. Gutjahr, S. Kowalewski, D. Hartz, H.D. Summ, Biochim. Biophys. Acta 1191 (1994) 278–290.
[29] G. Muller, D. Hartz, J. Punter, R. Okonomopulos, W. Kramer, Biochim. Biophys. Acta 1191 (1994) 267–277.
[30] K. Hastedt, U. Panten, Biochem. Pharmacol. 65 (2003) 599–602.
[31] S. Hu, S. Wang, B. Fanelli, P.A. Bell, B.E. Dunning, S. Geisse, R. Schmitz, B.R. Boettcher, J. Pharmacol. Exp. Ther. 293 (2000) 444–452.
[32] H. Weber, W. Aumuller, K. Muth, R. Weyer, Benzenesulfonyl ureas, 1976 US patent 3932503.
[33] H. Weber, W. Aumuller, R. Weyer, K. Muth, F.H. Schmidt, Benzenesulfonyl ureas and process for their manufacture, 1969 US patent 3426067.
[34] H. Weber, W. Aumuller, K. Muth, R. Weyer, R. Heerdt, E. Fauland, A. Bander, W. Pfaff, F.H. Schmidt, H. Stork, Arzneim-Forsch. 19 (1969) 1346–1362.
[35] J. Buckingham (ed.), Dictionary of Organic Compounds, Chapman and Hall, New York, 1982.
[36] B.S. Furniss, A.J. Hannaford, P.W.G. Smith, A.R. Tatchell, Vogel's Textbook of Practical Organic Chemistry, Longman Scientific & Technical, London, 1989.
[37] Hilton-Davis, US patent 4874894, 1989.
[38] I. Fabricius, GB patent 11885013, 1970.
[39] G.R. Brown, A.J. Foubister, J. Med. Chem. 27 (1984) 79–81.
[40] U. Burkert, N.L. Allinger, Molecular Mechanics, ACS, Washington, DC, 1982.
[41] N.L. Allinger, X. Zhou, J. Bergsma, J. Mol. Struct. (Theochem) 312 (1994) 69–83.
[42] J. Kao, C. Eyermann, E. Southwick, D. Leister, J. Am. Chem. Soc. 107 (1985) 5324.
[43] D.L. Mattern, X. Chen, J. Org. Chem. 56 (1991) 5903–5907.
[44] J.B. Nicholas, R. Vance, E. Martin, B.J. Burke, A.J. Hopfinger, J. Phys. Chem. 95 (1991) 9803–9811.